Journal of the Korean Ceramic Society
Vol. 55, No. 5, pp. 504–509, 2018.

https://doi.org/10.4191/kcers.2018.55.5.10

Yttrium Doping Effect on Varistor Properties of Zinc-Vanadium-Based Ceramics

Choon-W. Nahm†

Semiconductor Ceramics Laboratory, Department of Electrical Engineering, Dongeui University, Busan 47340, Korea

(Received June 28, 2018; Revised August 22, 2018; Accepted August 23, 2018)

ABSTRACT

The influence of yttrium doping on varistor properties of zinc-vanadium-based ceramics was comprehensively investigated. The average grain size varied slightly between 5.2 and 5.5 μm as the yttrium content increased; and similarly, the sintered density varied slightly between 5.47 and 5.51 g/cm^3. The threshold field exhibited a maximum value (5387 V/cm) when the yttrium content was 0.1 mol%. The highest nonlinear exponent (67) was obtained when the yttrium content was 0.05 mol%. The donor concentration increased in the range of (2.46–5.56) × 10^{17} cm^{-3} as the yttrium content increased, and the maximum barrier height was obtained (1.24 eV) when the yttrium content reached 0.05 mol%.

Key words : Yttrium, Dielectric properties, Electrical properties, Zinc-vanadium-based ceramics

1. Introduction

A varistor is a voltage-dependent resistor or nonlinear resistor. Unlike a general resistor, its resistance changes according to the applied voltage. Materials exhibiting a varistor effect must have a microstructure such as a pn junction or an active grain boundary or an active interface. Zinc oxide varistors are made by adding several specified additives to zinc oxide and firing it at a proper temperature.[1,2] The microstructure of doped zinc oxide varistors is a polycrystalline composed of numerous semiconducting zinc oxide grains and grain boundaries. The grains are semiconductors with a band gap of ~ 3.2 eV, and the grain boundaries are active for electrons and have a very thin insulating layer. As a result, one semiconductor–insulating layer–semiconductor (SIS) structure yields a microvaristor. Microvaristors are randomly distributed throughout a sintered body. Consequently, sintering zinc oxide doped with specified minor additives produces a distinctive microstructure and nonlinear conduction properties. Owing to the superior nonlinearity of zinc oxide varistors, they can be effectively applied to bypass various passive and active devices, protect electrical and electronic equipment from dangerous transient voltages, and protect electric facilities from lightning.[1,3]

Today, most varistors are doped mainly with bismuth and partially with praseodymium.[4,5] Because these varistor ceramics should be fired at a temperature higher than 1000°C, expensive Pd or Pt is inevitably used for multilayering.[6] Moreover, Ag, with its excellent conductivity, can be used as an inner electrode. Therefore, at this time, varistor ceramics that can be co-fired at a temperature lower than the melting point (960°C) of Ag are required, making vanadium-doped zinc oxide ceramics suitable here.[7,8]

Since 1994,[7] vanadium-doped zinc oxide varistors have been continuously studied.[9–16] Despite considerable improvements, however, they are still inadequate for practical use.[14,17–19] Nahm first reported that zinc-vanadium varistors doped with manganese–niobium oxides exhibited highly nonlinear properties.[20] On the basis of this composition, it was found that gadolinium additives significantly improved the nonlinearity of zinc-vanadium-based varistor ceramics.[21] Obtaining better varistor characteristics requires ongoing study.

In this work, we investigate the influence of yttrium dopants on the microstructure and electrical and dielectric characteristics of yttrium-doped zinc-vanadium-based ceramics and report a considerably high nonlinear exponent ($\alpha = 67$) for varistor ceramics.

2. Experimental Procedure

2.1. Specimen preparation

The composition formula for the specimens is as follows: $(97.4 - x)ZnO + 0.5V_2O_5 + 2.0MnO_2 + 0.1Nb_2O_5 + xY_2O_3$ (where x = 0.0, 0.05, 0.1, and 0.25) (all in mol%). The specimens were prepared in the following order using the traditional ceramic technique: The raw material was balanced with the composition expression and then ball milled for 24 h together with acetone as a dispersion medium. The mixture was dried at 120°C and granulated with a polyvinyl butyral (PVB) binder to use as a starting powder. The granulated powder was pressed into 1.5 mm thick disks of 10 mm diameter, under a pressure of 1000 kg/cm^2. The disks

†Corresponding author : Choon-W. Nahm
E-mail : cwnahm@deu.ac.kr
Tel : +82-51-890-1669 Fax : +82-505-182-6900

were set onto a magnesia plate and fired at 900°C for 3 h. Lapping and polishing produced final disks of 8 mm diameter and 1.0 mm thickness. The surfaces of the disks were painted with a conductive silver paste, to use as electrodes, and then fired at 550°C for 10 min.

2.2. Microstructure analysis

The fracture microstructure images of the sintered disks were examined under a field emission scanning electron microscope (Quanta 200). The average grain size d was calculated using the expression d = 1.56 L/MN proposed by Wurst *et al.*[22] The phases of the sintered specimens were identified by X-ray diffraction (XRD) patterns using CuKα radiation (X'pert–PRO MPD). The sintered densities r were measured by using a density determination kit (238490) attached to a balance (AG 245).

2.3. J–E characteristics measurement

The current–voltage (I–V) characteristics were automatically measured using a high-voltage source-measure unit (Keithley 237). The I–V characteristics are converted to current density–electric field (J–E) characteristics. The threshold voltage $V_{1\ mA/cm^2}$ was measured at 1.0 mA/cm^2. The leakage current I_L was measured at 0.8 $V_{1\ mA/cm^2}$. The threshold field $E_{1\ mA/cm^2}$, the nonlinear exponent α, and the leakage current density J_L are calculated from $E_{1\ mA/cm^2} = V_{1\ mA/cm^2}/D$, $\alpha = 1/\log(V_{10\ mA/cm^2}/V_{1\ mA/cm^2})$, and $J_L = I_L/S$, respectively, where D is the thickness of the specimens (1 mm) and S is the area of the electrodes.

The capacitance–voltage (C–V) characteristics were measured at a frequency of 1 kHz and a bias voltage in the 0–100 V range by using a precision LCR meter (QuadTech 7600) and an electrometer (Keithley 617) in a DC source. The donor concentration N_d and the barrier height Φ_b were determined from the expression $(1/C_b - 1/2C_{bo})^2 = 2(\Phi_b + V_{gb})/q\varepsilon N_d$ proposed by Mukae *et al.*[23] The interface state density N_t between the grain and the intergranular layer in the grain boundary was calculated from the expression[23] $N_t = (2\varepsilon N_d \Phi_b/q)^{1/2}$.

2.4. Dielectric characteristics measurement

The apparent capacitance C_{APP}' and dissipation factor tanδ were measured from 10 Hz to 1 MHz by using an RLC meter (QuadTech 7600). The dielectric constant ε_{APP}' was calculated from $C_{APP}' = \varepsilon_{APP}' S/D$.

3. Results and Discussion

Figure 1 presents the surface microstructures of ZnO ceramics doped with several yttrium contents. Seemingly, there is no detectable difference on the surface between the yttrium-free ZnO ceramics and the yttrium-doped ZnO ceramics. On the whole, the phase distribution is homogeneous. The average grain size d according to the yttrium content is presented in Fig. 2. As the yttrium content increased, the average grain size d decreased slightly from

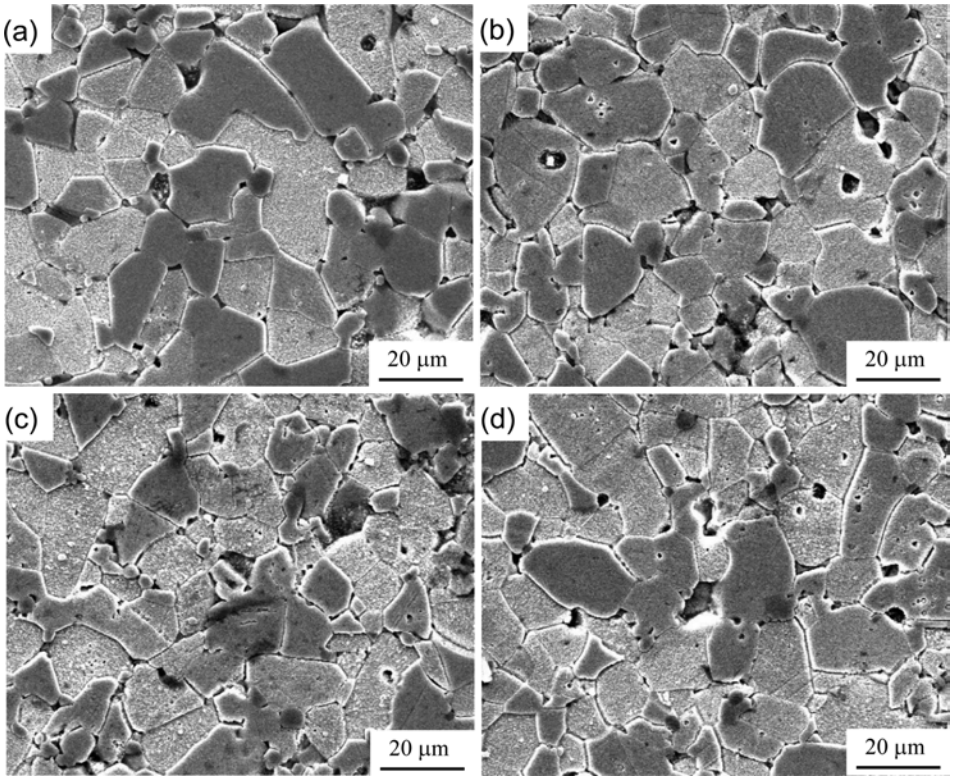

Fig. 1. Scanning electron microscope micrographs of ZnO ceramics doped with yttrium contents of (a) 0.0 mol%, (b) 0.05 mol%, (c) 0.1 mol%, and (d) 0.25 mol%.

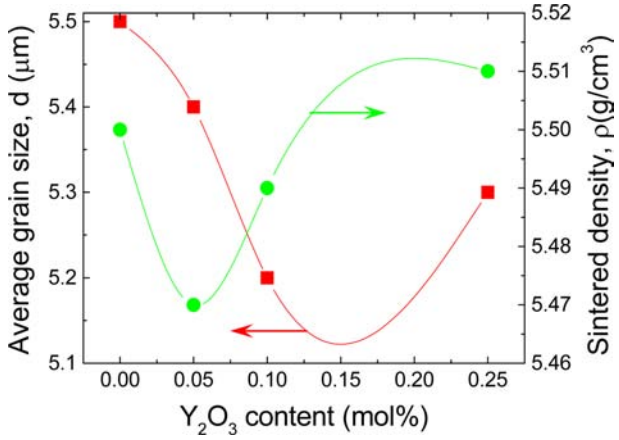

Fig. 2. Average grain size and sintered density of ZnO ceramics as a function of yttrium content.

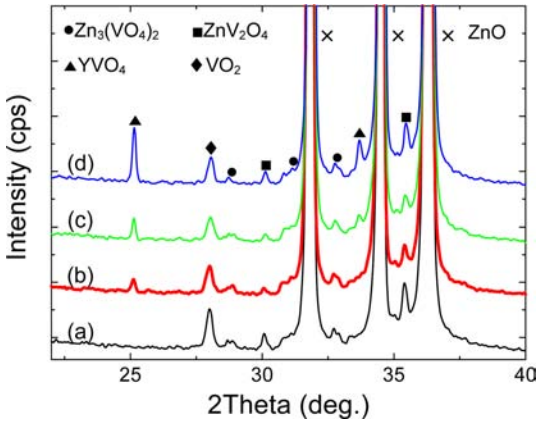

Fig. 3. XRD patterns of ZnO ceramics doped with yttrium contents of (a) 0.0 mol%, (b) 0.05 mol%, (c) 0.1 mol%, and (d) 0.25 mol%.

5.5 to 5.2 μm until the yttrium content reached 0.1 mol%. When the yttrium content exceeded 0.1 mol%, the average grain size d increased to 5.3 μm. However, the change of the average grain size d according to the yttrium content is not very great. The decrease in the average grain size d is ascribed to the increase of YVO_4 generated by doping with yttrium (see Fig. 3). The sintered density ρ according to the yttrium content is presented in Fig. 2. The sintered density ρ decreased slightly up to 0.05 mol%, whereas a further increase in the yttrium content increased the sintered density ρ in the range of 5.47–5.51 g/cm^3. As the yttrium content increased, the change of the sintered density ρ, like the average grain size d, is not great. On the whole, the influence of yttrium doping on the microstructure is minor, when compared with other.[21] A few microstructure parameters for several yttrium contents are summarized in Table 1.

Figure 3 presents the typical XRD patterns of ZnO ceramics doped with several yttrium contents. All the specimens revealed minor phases such as VO_2, ZnV_2O_4, and $Zn_3(VO_4)_2$. The specimens doped with yttrium generated YVO_4 as a minor phase.

Figure 4 presents the J–E characteristics of ZnO ceramics doped with several yttrium contents. The J–E characteristics comprise a high-impedance region below the knee voltage and a low-impedance region above the knee voltage. The distribution of J–E curves shows that yttrium doping greatly affects the nonlinearity. With increasing yttrium content, the threshold field $E_{1\ mA/cm^2}$ increased in the range of 4874–5387 V/cm when the yttrium content reached 0.1 mol%. When the yttrium content exceeded 0.1 mol%, the threshold field $E_{1\ mA/cm^2}$ decreased up to 5355 V/cm at 0.25 mol% yttrium. The behavior of the threshold field $E_{1\ mA/cm^2}$ with increasing yttrium content depends on the average grain size d. The decrease in the average grain size brings about an increase of the number of grain boundaries. All the specimens exhibited v_{gb} = 2.7–2.8 V/(grain boundary) for the threshold voltage per grain boundaries regardless of the yttrium content.

The nonlinear exponent α according to the yttrium content is presented in Fig. 5. The J–E curves in varistor ceramics all feature a nonlinear exponent α. As the yttrium content increased, the nonlinear exponent α increased pronouncedly from 51 to 67, until the yttrium content reached 0.05 mol%. When the yttrium content exceeded 0.05 mol%, the nonlinear exponent α decreased up to 40 at 0.25 mol% yttrium. The specimen doped with 0.05 mol% yttrium exhibited the largest α (α = 67) of the ZnO–V_2O_5 systems known so far.[21] The abrupt decrease of the nonlinear exponent α at 0.25 mol% in the yttrium content is ascribed to the decrease in the potential barrier height at the grain boundaries. Basically, the potential barrier is affected by various defects (interstitial zinc, interstitial oxygen, zinc vacancies, etc.) at the grain boundary.[24,25] Therefore, the nonlinear exponent α is strongly affected by the Schottky barrier. However, the behavior of the nonlinear exponent a according to the yttrium content may be connected with the content of $YbVO_4$. That is, YVO_4-free or excess YVO_4 can reduce the nonlinear exponent α. The leakage current density J_L

Table 1. Microstructure and Electrical Characteristic Parameters of ZnO Ceramics Doped with Several Yttrium Contents

Yttrium content (mol%)	d (μm)	ρ (g/cm^3)	$E_{1\ mA/cm^2}$ (V/cm)	v_{gb} (V/grain boundary)	a	J_L (μA/cm^2)
0.0	5.5	5.50	4874	2.7	51	56.8
0.05	5.4	5.47	4989	2.7	67	99.7
0.1	5.2	5.49	5387	2.8	53	105.5
0.25	5.3	5.51	5355	2.8	40	251.6

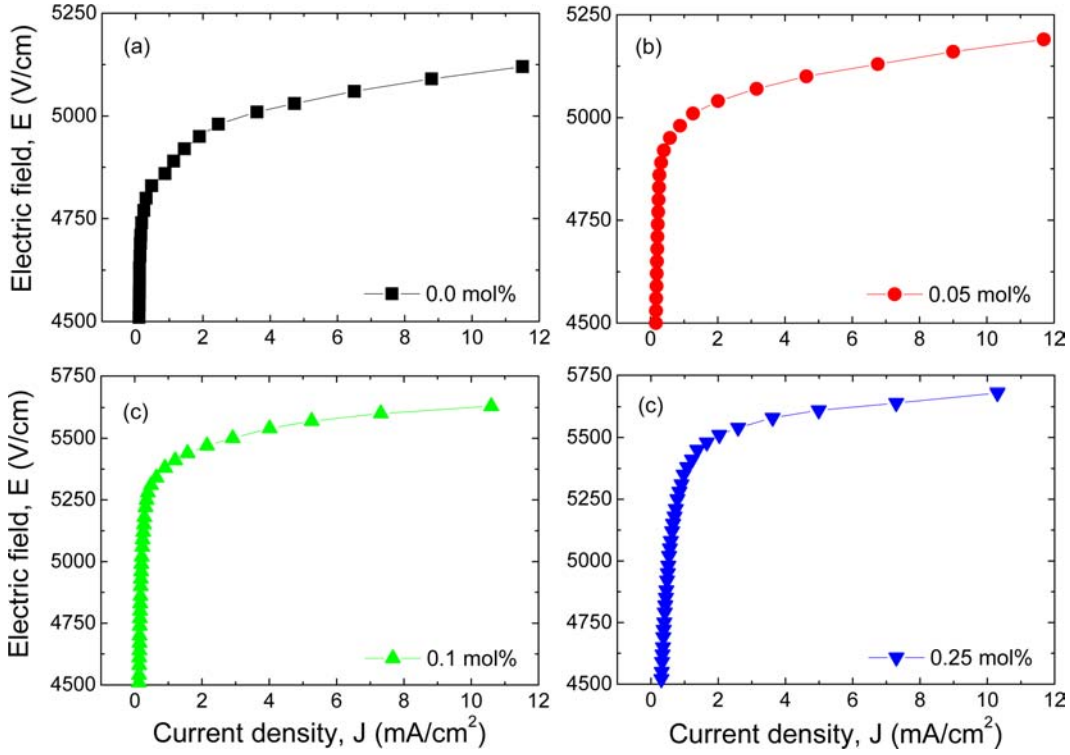

Fig. 4. *J–E* characteristics of ZnO ceramics doped with several yttrium contents.

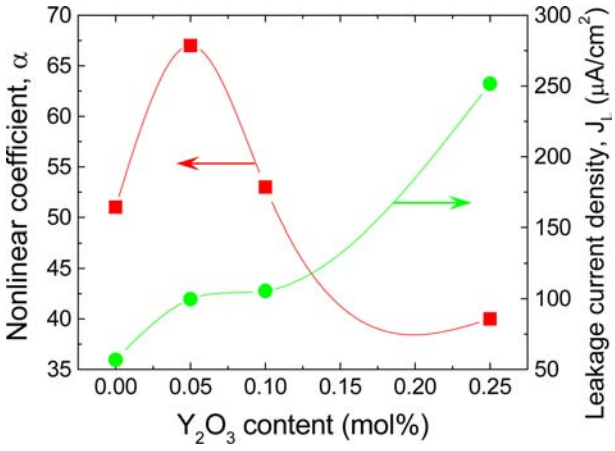

Fig. 5. Nonlinear exponent and leakage current density of ZnO ceramics as a function of yttrium content.

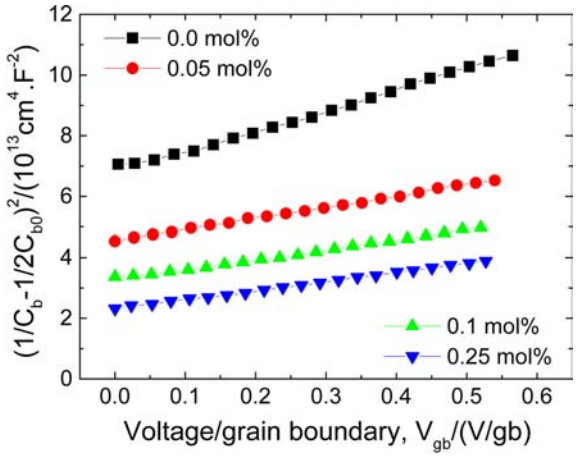

Fig. 6. *C–V* characteristics of ZnO ceramics doped with several yttrium contents.

according to the yttrium content is presented in Fig. 5. As the yttrium content increased, the leakage current density J_L increased from 56.8 to 251.6 μA/cm^2. A few *J–E* characteristic parameters with several yttrium contents are listed in Table 1. These results verify that yttrium doping much more greatly affects *J–E* characteristics than the microstructure.

Figure 6 presents the modified capacitance–voltage (*C–V*) characteristic graphs of ZnO ceramics doped with several yttrium contents. A few *C–V* characteristic parameters with several yttrium contents are summarized in Table 2. As the yttrium content increased, the donor concentration N_d increased from 2.46×10^{17} to 5.56×10^{17} cm^{-3}. The yttrium dopant seems to act as a donor, based on the chemical-defect reaction $Y_2O_3 \xrightarrow{ZnO} 2Y_{Zn}^{\cdot} + 2O_O + \frac{1}{2}O_2 + 2e'$.

As the yttrium content increased, the barrier height Φ_b increased in the range of 1.01–1.24 eV, until the yttrium content reached 0.05 mol%. However, when the yttrium content was > 0.05 mol%, Φ_b decreased to 0.77 at 0.25 mol% yttrium. As the yttrium content increased, the tendency of change in Φ_b coincided with the tendency of the nonlinear exponent in the *J–E* characteristics. In general, the higher the value of Φ_b, the better the nonlinear properties. Meanwhile, the tendency of change in the interface state density

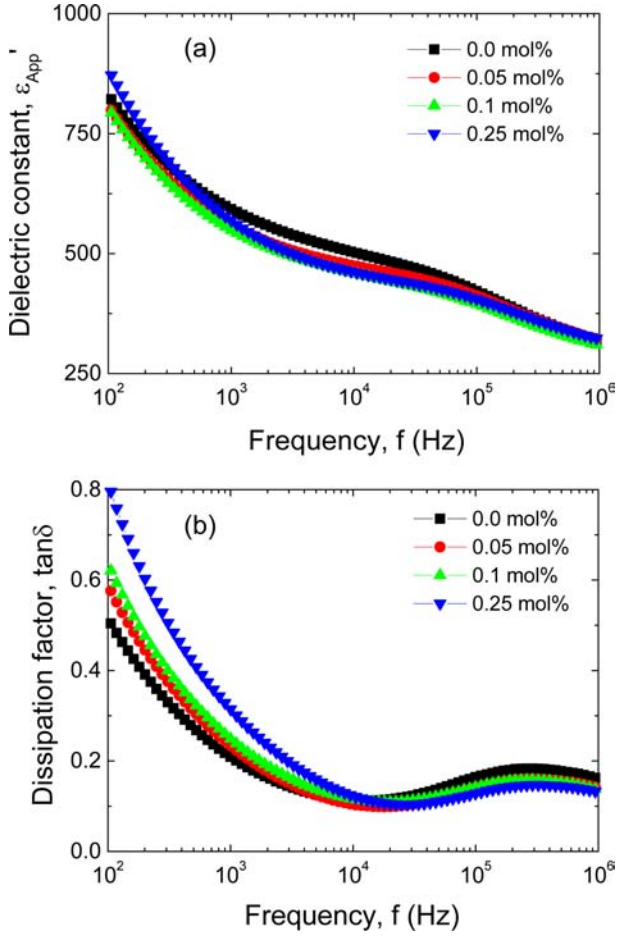

Fig. 7. Dielectric characteristics of ZnO ceramics doped with several yttrium contents: (a) dielectric constant ε_{APP}' and (b) dissipation factor tand.

N_t coincided with the tendency of Φ_b according to the yttrium content. The barrier height is closely connected to the interface state density.

Figure 7 presents the dielectric characteristics of ZnO ceramics doped with several yttrium contents. Fig. 7(a) shows that the dielectric constant ε_{APP}' decreased with an abrupt drop at < 1 kHz and with a gradual drop at > 100 kHz when the frequency increased. On the whole, as shown through the curves, the influence of yttrium doping on the dielectric constant ε_{APP}' is not significant, when compared with other.[21] The behavior of the dielectric constant ε_{APP}' (at 1 kHz) according to the yttrium content is presented in Fig. 8. As the yttrium content increased, the dielectric constant

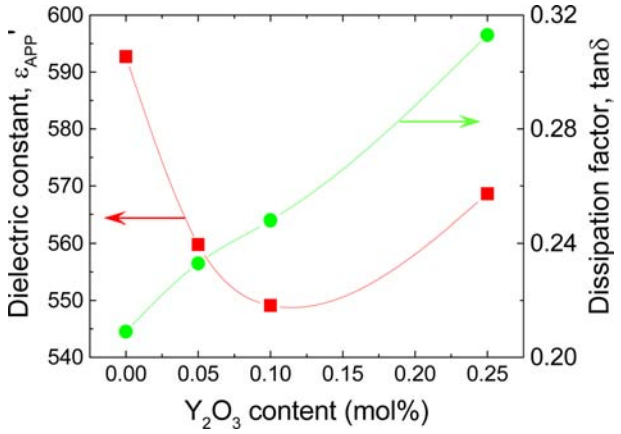

Fig. 8. Dielectric constant and dissipation factor of ZnO ceramics as a function of yttrium content.

ε_{APP}' (at 1 kHz) decreased from 592.7 to 549.1 until the yttrium content reached 0.1 mol%. When the yttrium content exceeded 0.1 mol%, the dielectric constant ε_{APP}' increased up to 568.6 at 0.25 mol% yttrium. This trend in the value of the dielectric constant ε_{APP}' is deeply related to the microstructure.

Meanwhile, as shown in Fig. 7(b), the dissipation factor tanδ decreased abruptly up to ~ 20 kHz in all the specimens. All the specimens revealed an absorption peak at ~ 300 kHz, which decreased again when the frequency exceeded 300 kHz. The variation in the dissipation factor tanδ (at 1 kHz) according to the yttrium content is presented in Fig. 8. The dissipation factor tanδ increased in the range of 0.209–0.313 with increasing yttrium content. This trend in the value of the dissipation factor tanδ is closely connected with the leakage current. On the whole, it is assumed that the high dissipation factor tanδ in all the specimens is ascribed to a relatively high leakage current. A few dielectric parameters with several yttrium contents are listed in Table 2.

4. Conclusions

The varistor properties of zinc-vanadium-based ceramics were comprehensively investigated at 0–0.25 mol% yttrium contents. The influence of yttrium doping on the microstructure of varistor ceramics was not as large compared with others with the same doping content: The average grain size was in the narrow range of 5.2–5.5 μm and the sintered density was in the narrow range of 5.47–5.51 g/cm^3. However,

Table 2. *C–V* and Dielectric Characteristic Parameters of ZnO Ceramics Doped with Several Yttrium Contents

Yttrium content (mol%)	N_d (10^{17} cm^{-3})	Φ_b (eV)	N_t (10^{12} cm^{-2})	ε_{APP} (1 kHz)	tanδ (1 kHz)
0.0	2.46	1.01	1.53	592.7	0.209
0.05	4.53	1.24	2.30	559.8	0.233
0.1	5.18	1.03	2.23	549.1	0.248
0.25	5.56	0.77	2.01	568.6	0.313

the nonlinear properties were greatly affected by small changes in yttrium content. The largest effect of yttrium doping on the nonlinear properties was observed when the yttrium content was 0.05 mol%. The yttrium dopant played the role of a donor, as evident by the increase in electron concentration with increasing yttrium content. It is concluded that zinc-vanadium-based ceramics doped with appropriate yttrium content can be expected to contribute to the development of chip varistors.

REFERENCES

1. L. M. Levinson and H. R. Philipp, "Zinc Oxide Varistor-a Review," *Am. Ceram. Soc. Bull.*, **65** [4] 639–46 (1986).
2. T. K. Gupta, "Application of Zinc Oxide Varistor," *J. Am. Ceram. Soc.*, **73** [7] 1817–40 (1990).
3. H. R. Pilipp and L. M. Levinson, "The Physics of Metal Oxide Varistors," *J. Appl. Phys.*, **46** [3] 1332–41 (1976).
4. M. Matsuoka, "Nonohmic Properties of Zinc Oxide Ceramics," *Jpn. J. Appl. Phys.*, **10** [6] 736 (1971).
5. K. Mukae, "Zinc Oxide Varistors with Praseodymium Oxide," *Am. Ceram. Bull.*, **66** [10] 1329–31 (1987).
6. C.-W. Nahm and C.-H. Park, "Microstucture, Electrical Properties, and Degradation Behavior of Praseodymium Oxides-based Zinc Oxide Varistors Doped with Y_2O_3," *J. Mater. Sci.*, **35** [12] 3037–42 (2000).
7. J.-K. Tsai and T.-B. Wu, "Non-Ohmic Characteristics of ZnO-V_2O_5 Ceramics," *J. Appl. Phys.*, **76** [8] 4817–22 (1994).
8. J.-K. Tsai and T.-B. Wu, "Microstructure and Nonohmic Properties of Binary ZnO-V_2O_5 Ceramics Sintered at 900°C," *Mater. Lett.*, **26** [3] 199–203 (1996).
9. H.-H. Hng and P. L. Chan, "Effects of MnO_2 Doping in V_2O_5-Doped ZnO Varistor System," *Mater. Chem. Phys.*, **75** [1–3] 61–6 (2002).
10. C.-S. Chen, "Effect of Dopant Valence State of Mn-ions on the Microstructures and Nonlinear Properties of Microwave Sintered ZnO-V_2O_5 Varistors," *J. Mater. Sci.*, **38** [5] 1033–38 (2003).
11. H. Pfeiffer and K. M. Knowles, "Effects of Vanadium and Manganese Concentrations on the Composition, Structure and Electrical Properties of ZnO-rich MnO_2-V_2O_5-ZnO Varistors," *J. Eur. Ceram. Soc.*, **24** [6] 1199–203 (2004).
12. C.-W. Nahm, "Microstructure and Varistor Properties of ZnO-V_2O_5-MnO_2-Based Ceramic," *J. Mater. Sci.*, **42** [19] 8370–73 (2007).
13. M. Zhao, X. C. Liu, W. M. Wang, F. Gao, and C. S. Tian, "Two-step Method Fabricating High Nonlinearity ZnVSb Based Varistors," *Ceram. Int.*, **34** [6] 1425–29 (2008).
14. C.-W. Nahm, "Influence of Nb Addition on Microstructure, Electrical, Dielectric Properties, and Aging Behavior of MnCoDy Modified Zn-V-Based Varistors," *J. Mater. Sci.: Mater. Electron.*, **21** [6] 540–47 (2010).
15. Z. Ming, S. Yu, and T. C. Sheng, "Grain Growth of ZnO–V_2O_5 Based Varistor Ceramics with Different Antimony Dopants," *J. Eur. Ceram. Soc.*, **31** [13] 2331–37 (2011).
16. M. Mirzayi and M. H. Hekmatshoar, "Effect of V_2O_5 on Electrical and Microstructural Properties of ZnO Ceramics," *Phys. B*, **414** [4] 50–5 (2013).
17. C.-W. Nahm, Sintering Effect on Pulse Aging Behavior of Zn-V-Mn-Co-Nb Varistors. *J. Am. Ceram. Soc.*, **94** [8] 2269–72 (2011).
18. C.-W. Nahm, "DC Accelerated Aging Behavior of Co-Dy-Nb Doped Zn-V-M-Based Varistors with Sintering Process," *J. Mater. Sci.: Mater. Electron.*, **22** [4] 444–51 (2011).
19. C.-W. Nahm, "Aging Characteristics of ZnO-V_2O_5-based Varistors for Surge Protection Reliability," *Microelectron. Reliab.*, **54** [12] 2836–42 (2014).
20. C.-W. Nahm, "Effect of Sintering Process on Electrical Properties and Ageing Behavior of ZnO-V_2O_5-MnO_2-Nb_2O_5 Varistor Ceramics," *J. Mater. Sci.: Mater. Electron.*, **23** [2] 457–63 (2012).
21. C.-W. Nahm, "Effect of Gadolinia Addition on Varistor Characteristics of Vanadium Oxide–Doped Zinc Oxide Ceramics," *J. Mater. Sci.: Mater. Electron.*, **24** [12] 4839–46 (2013).
22. J. C. Wurst and J. A. Nelson, "Lineal Intercept Technique for Measuring Grain Size in Two-Phase Polycrystalline Ceramics," *J. Am. Ceram. Soc.*, **55** [97–12] 109–11 (1972).
23. M. Mukae, K. Tsuda, and I. Nagasawa, "Capacitance-vs-voltage Characteristics of ZnO Varistor," *J. Appl. Phys.*, **50** [6] 4475–76 (1979).
24. G. D. Mahan, "Intrinsic Defects in ZnO Varistors," *J. Appl. Phys.*, **54** [7] 3825–32 (1983).
25. T. K. Gupta and W. G. Carlson, "A Grain-boundary Defect Model for Instability/Stability of a ZnO Varistor," *J. Mater. Sci.*, **20** [3] 3487–500 (1985).